SciEn

Proceedings of 8th International Conference on Mechanical Engineering and Renewable Energy 2025
10-12 December, 2025, Chattogram, BANGLADESH

SciEn Conference Series: Engineering Vol. 4, 2026, pp 636-641 https://doi.org/10.38032/scse.2026.4.293

NiO and Co-Doped NiO Multifunctional Nanomaterials: Biogenic Fabrication for Enhanced Photocatalytic Activity.

Shah Sadia Rahman Joya, Md. Estabrak Ahammod Sakib, Md. Lael Hasan, Hridoy Roy, and Md. Farhan Muskan*

Department of Ceramic & Metallurgical Engineering, Rajshahi University of Engineering & Technology, Rajshahi-6204.

ABSTRACT

Biogenically synthesized NiO and Co-doped NiO nanoparticles were fabricated using Rosella fruit extract as a natural reducing and capping agent. Structural analysis confirmed a cubic lattice with successful Co incorporation, resulting in a reduction of crystallite size from 10.73 nm to 8.93 nm and an increase in dislocation density. SEM imaging revealed agglomerated cubic morphologies, while EDS certified the elemental purity of Ni, O, and Co. UV-Visible spectroscopy showed a red-shifted absorption edge and band gap narrowing from 3.15 eV to 2.72 eV, favoring electron excitation. FTIR spectra confirmed the presence of metal-oxygen bonding and functional groups associated with the extract. Photocatalytic testing demonstrated the enhanced performance of Co-NiO, with 95.58% degradation of methylene blue, correlating with structural refinement and optical band tailoring. These findings demonstrate the effectiveness of Co substitution in modulating the microstructure and optoelectronic properties of NiO nanoparticles for advanced photocatalytic applications.

Keyword: Biogenic Synthesis, Rosella Fruit, Photocatalytic Activity, Dye degradation.

1. Introduction

Organic pollutants or dyes are among the most harmful sources of water contamination. [1]. Several technologies have been applied to filter water, including the use of instruments based on inexpensive adsorbents, with a particular focus on nano-sized metal oxide photocatalysts [1], [2], [3]. These photocatalysts are widely studied and used for promoting the deprivation of organic dyes, such as Methylene Blue (MB) and Rhodamine B dye. Moreover, metal oxide nanoparticles possess unique chemical and physical properties that have attracted significant attention in the field of science [4], [5].

Transition metal oxide nanoparticles, such as MnO, CoO, FeO, CuO, ZnO, and NiO, are wide-bandgap semiconductors. They are electrically insulating, exhibit excellent electrochemical stability, and display antiferromagnetic behavior [6], [7], which makes them unique in science with diverse applications including Li-ion batteries, supercapacitors, optoelectronic devices, gas sensors, solar cells, electrochromic displays, magnetic materials, catalysts, and biomedical devices [6], [8]. Among them, NiO nanoparticles have gained considerable attention due to their low cost, high durability, excellent chemical stability, and ease of fabrication [8], [9]. In addition, NiO is a p-type semiconductor with a wide band gap in the range of 3.6–4.0 eV, which makes it highly suitable as a catalyst [10], [11], [12].

Doping is a common technique to enhance the properties of pure metal oxide nanoparticles and to discover new materials for technological applications. Transition metals such as Mn, Fe, Ni, Ti, Cu, Co, and Zn are suitable dopants for improving these properties [13]. Among them, Co is particularly suitable for doping into NiO nanoparticles due to its similar ionic radius, high solubility, and favorable luminescence activity [8], [13].

Several methods have been used for the fabrication of metal oxide nanomaterials, including sol-gel, hydrothermal, solvothermal, chemical combustion, biogenic synthesis, co-precipitation, solid-state reaction, laser-assisted chemical methods, and microwave-assisted synthesis [7], [8], [14]. Among these, biogenic synthesis has become more popular because it is cost-effective, eco-friendly, and non-toxic [15]. Roselle fruit (*Hibiscus sabdariffa* L.) has been used as a green source during synthesis, providing flavonoids, anthocyanins, and pectin, which act as capping and reducing agents [16].

Previous studies have highlighted the versatile applications of doped NiO nanoparticles. For instance, 10% Co-doped NiO nanoparticles synthesized via co-precipitation exhibited remarkable efficiency in wastewater treatment [17]. Similarly, Ce-doped NiO nanoparticles (1% and 3%) prepared by co-precipitation achieved significant degradation of Rhodamine B dye, reaching efficiencies of 85.99% and 94.06%, respectively [5]. In another investigation, $Co_xNi_{1-x}O$ (x = 0, 0.01, 0.03, 0.05, and 0.10) nanoparticles were explored to reveal novel functional properties, marking one of the first comprehensive reports in this domain [8]. Furthermore, $Co_xNi_{1-x}O$ (x = 0.0, 0.1, 0.2, 0.3, 0.4) nanoparticles demonstrated room-temperature ferromagnetic behavior [18], while $Co_xNi_{1-x}O$ (x = 0, 0.03, 0.07, 0.10, 0.13, 0.15) nanoparticles exhibited distinct fluorescence characteristics [6].

In this study, 5% cobalt (Co) was doped into NiO and fabricated via a biogenic synthesis approach. The structural,

*Corresponding Author Email Address: sadia.joya@cme.ruet.ac.bd

morphological, and optical properties of the nanoparticles were evaluated through X-ray diffraction (XRD), scanning electron microscopy (SEM), and UV–visible spectroscopy, respectively. The functional groups were identified using Fourier transform infrared (FTIR) spectroscopy. The primary objective of this study was to enhance the photocatalytic activity of the nanoparticles, thereby contributing to the mitigation of environmental pollution.

2. Experimental Details

2.1. Materials

Nickel nitrate hexahydrate ($Ni(NO_3)_2 \cdot 6H_2O$, Purity: 98.5%, Origin: Merck, India) as a source of Ni, cobalt chloride hexahydrate ($CoCl_2 \cdot 6H_2O$, Purity: 99.99%, Origin: Merck, Germany) as a source of Co, and NaOH hydroxide (NaOH, Purity: 99.0%, Origin: India) were used for producing the nanomaterials. Di-ionized water was used for the solution formulation throughout the research. All raw materials used in this experiment were of analytical grade.

2.2. Preparation of Nanoparticles

Green objects (Rosella fruits) were collected from the local area of Rajshahi, thoroughly washed with distilled water, and boiled in 250 mL of deionized water at 60℃ for 30 minutes. The resulting extract was then cooled at room temperature and filtered through Whatman No. 1 filter paper to obtain a final solution of the extract.

During NiO nanoparticle fabrication, 100 mL of a 0.5 M nickel nitrate hexahydrate solution was prepared by dissolving the nickel nitrate hexahydrate in deionized water. 50 mL of extract was added dropwise to the nickel salt solution and magnetically stirred at 65 °C for 60 minutes, resulting in a visible color change and the formation of NiO nanoparticles. After that, the solution was centrifuged, washed twice with a 15% ethanol solution, dried overnight at 100℃, and then calcined at 450℃ for 1.5 hours to obtain the desired NiO nanoparticles. For Co-doped NiO nanoparticles, 0.5M salt was taken in the section of 5% of cobalt chloride hexahydrate (0.595 g), and 95% of nickel nitrate hexahydrate (13.775 g) was dissolved in 100 mL of distilled water. Following this, a similar procedure was employed for NiO nanoparticle fabrication. In both cases, a 2 M NaOH solution was used to adjust the pH value to 10.

3. Result and Discussion

3.1. Structural Analysis

The structural properties and crystallite size of the samples were depicted using XRD analysis. Fig. 1 represents the structural pattern of both pure and Co-doped biogenically synthesized NiO nanoparticles. Sharp and intense peaks were observed within the 2Θ range of 30° - 80°. The diffraction peaks corresponding to the (111), (020), (022), (131), and (222) planes confirm the formation of nanoparticles [18], [19], [20], and indicate a face-centered cubic (FCC) structure with space group Fm-3m (225) [8], [17], [21]. All diffraction peaks of both pure and Co-doped NiO nanoparticles are well indexed with the standard JCPDS card no. 96-101-0096, with no evidence of secondary phases [8], indicating successful substitution of Co ions into the Ni ion lattice site without structural distortion [18], [22]. This is attributed to the nearly identical ionic radii of the Ni ion (0.69 Å) and Co ion (0.72 Å) [23].

Co-doping directed to a reduction in crystallite size, indicating restricted lattice growth [18] as calculated by the Debye-Scherrer equation [7].

$$d = \frac{k\lambda}{\beta \cos\theta} \quad (1)$$

Where D is the crystalline size, k is the Scherrer constant (0.98), λ is the wavelength (1.5403 nm), β denotes the full width at half maximum (FWHM) and θ = Bragg angle. The dislocation density of both nanoparticles was calculated using the corresponding equation (2) [5], showing an increase with decreasing crystallite size [5].

$$\delta = \frac{1}{D} \quad (2)$$

Where D is the crystallite size of the particles, and δ is the dislocation density. Table 1 summarizes all the structural parameters of the nanoparticles.

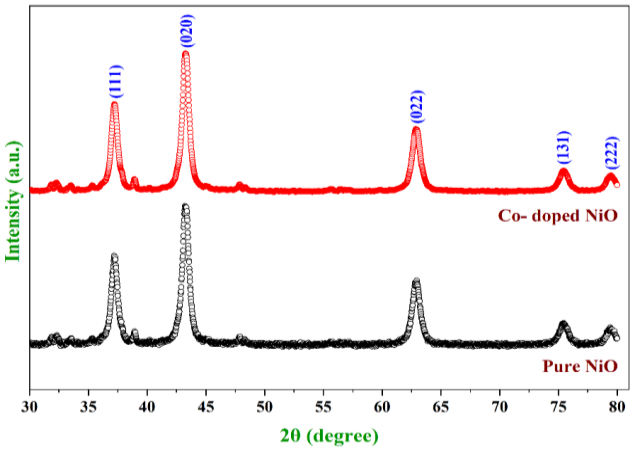

Fig.1 Structural pattern of the synthesized nanoparticles

Table 1 Structural parameters of synthesized NPs

Parameters	Nanomaterials	
	Pure NiO	Co-doped NiO
Crystallite Size, D (nm)	10.73	8.93
Dislocation Density, δ ($\times 10^{-4}$ nm^{-2})	86.85	125.40
Lattice Parameter (A°)	4.1790	4.1800
Cell Density (g/cm^3)	6.79	6.80
Unit Cell Volume (Å^3)	73.03	72.78

3.2. Morphological Analysis

Surface morphology and elemental composition of the synthesized nanoparticles were scrutinized using scanning electron microscopy (SEM) and energy dispersive X-ray spectroscopy (EDS). Fig. 2(a-b) shows the surface morphology of both pure and Co-doped NiO nanoparticles, revealing non-spherical [14], large cubic shapes with agglomerated [6] and non-uniform particle size [5], [24]. Such agglomeration is attributed to the nanoscale crystallite size and high surface-to-volume ratio [8], [14]. The grain size distribution presented in Fig. 2(a-b) demonstrates a reduction from 27.91 nm to 21.48 nm upon Co doping, indicating the suppression of lattice growth [5], [14]. Fig. 2(c-d) depicts the EDS spectra of pure NiO and Co-doped

NiO nanoparticles, where no extraneous peaks corresponding to foreign elements were detected. This analysis confirms the presence of Ni, O, and Co, verifying the successful incorporation of Co into the NiO lattice [5].

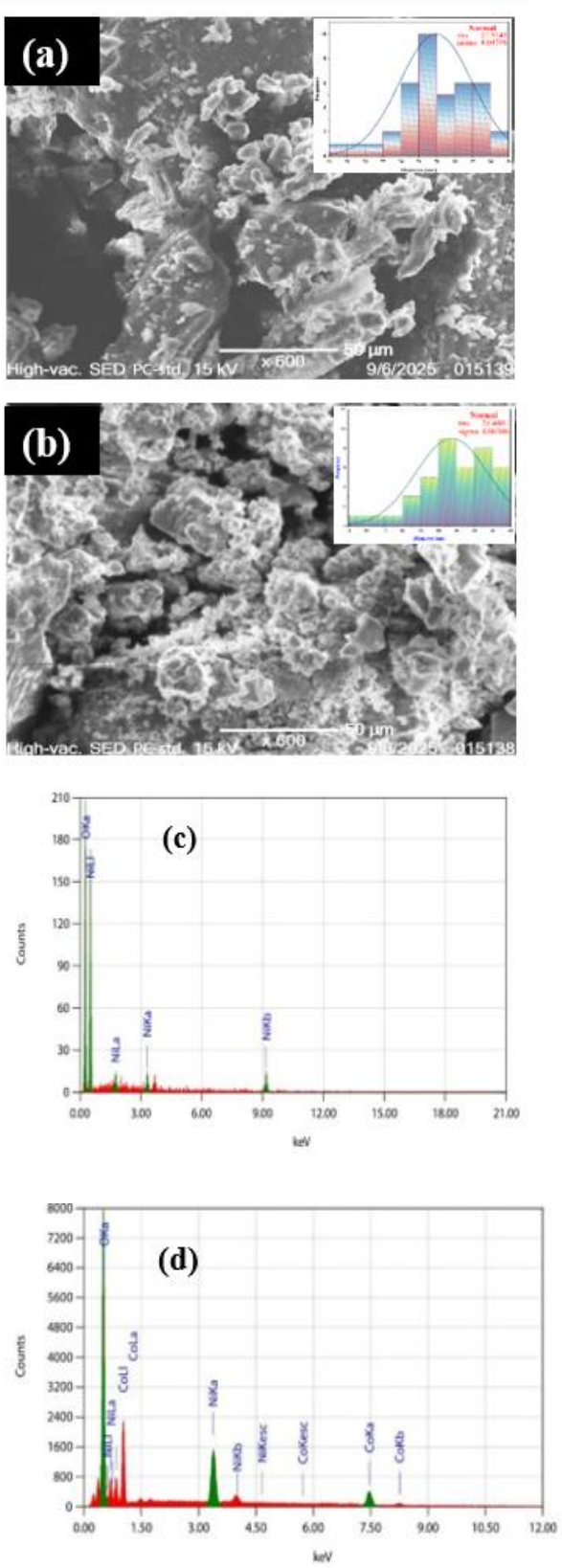

Fig.2 a) Morphological graph of Pure NiO, b) Morphological graph of Co-doped NiO, c) EDS graph of Pure NiO, and d) EDS graph of Co-doped NiO

3.3. Optical Analysis

The UV-visible absorption spectra of pure and Co-doped NiO nanoparticles are presented in Fig. 3a. A strong absorption peak at 264 nm and 268 nm, which exhibited a red shift upon the incorporation of Co into the pure NiO lattice structure [8]. The energy band gap of both nanoparticles was calculated using the following Tauc relation [25];

$$(\alpha h\vartheta) = [A(h\vartheta - Eg)]^n \quad (3)$$

Where α is the absorption coefficient, E_g is the band gap, A is a constant, υ is the transition frequency, and n assumes values of 1/2, 3/2, 2, or 3, for direct allowed, direct forbidden, indirect allowed, and indirect forbidden transition, respectively. The band gap was found to decrease from 3.15 eV to 2.72 eV (Fig. 3b), facilitating the excitation of electrons into the conduction band [5], [26], [27]. This reduction can be attributed to the substitution of Co ions within the NiO lattice [6], [8]. These values are consistent with previously reported results**.**

3.4. FTIR Analysis

To identify the chemical bonds and functional groups in the synthesized nanoparticles, FTIR spectra were recorded in the range of 4000 cm^{-1} to 500 cm^{-1}, as shown in Fig. 4. The sharp absorption peaks at 573 cm^{-1}, 626 cm^{-1}, and 691 cm^{-1} confirm the successful formation of NiO and Co-doped NiO nanoparticles [17]. The band at 626 cm^{-1} corresponds to metal-oxygen stretching vibrations at the tetrahedral site, while the peak at 573 cm^{-1} is attributed to metal-oxygen stretching at the octahedral sites [17]. A strong absorption peak at 3670 cm^{-1} is assigned to the O-H stretching vibration [8], [21], [28], indicating the presence of hydroxyl groups that may act as a reducing agent [17]. Additional peaks at 1496 cm^{-1} and 1263 cm^{-1} arise from the CH_2 stretching vibration of aromatic compounds [5], [29] and the asymmetric vibration of O=C=O, respectively [17], [29]. The band at 887 cm^{-1} is associated with aromatic C-H bending vibrations and intercalated C-O species [6], [17], [30].

3.5. Photocatalytic Activity Analysis

Figure 5(a–b) demonstrates the photocatalytic degradation of Methylene Blue (MB) as a function of irradiation time. As shown, appreciable dye degradation begins after 30 minutes, with the concentration of MB gradually decreasing as the degradation rate increases, accompanied by a visible lightening of the solution color. The degradation efficiency was calculated at the characteristic wavelength of 665 nm using the relation [17]:

$$Degradation\ (\%) = \frac{C_0 - C_t}{C_0} \times 100 \quad (4)$$

Where C_0 and C_t are the dye concentrations at the initial and irradiation time t, respectively, the band gap energies of 3.15 eV (pure NiO) and 2.72 eV (Co-doped NiO) expressively influenced the photocatalytic activity. The reduced band gap in Co-doped NiO facilitated enhanced light absorption, leading to a maximum degradation efficiency of 95.58%, which is higher than that of pure NiO (89.43%) [Fig. 5(a–b)]. This improvement can be attributed to the smaller particle size of Co-doped NiO, which provides a larger surface area and more active sites for dye adsorption [10], [17], [31]. Upon UV irradiation, electrons are excited from the valence band to the conduction band, leaving behind holes. These holes interact with water molecules to generate hydroxyl (•OH) radicals, which act as potent

oxidizing agents in the degradation process. The higher density of charge carriers in Co-doped NiO promotes the generation of more hydroxyl radicals, thereby accelerating dye degradation [32].

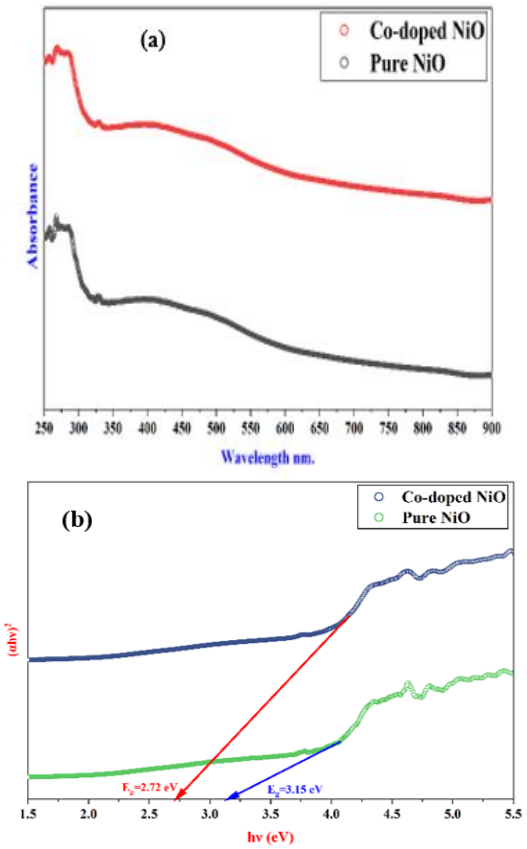

Fig.3 a) Absorbance graph of synthesized nanoparticles, b) Tauc plot of synthesized nanoparticles

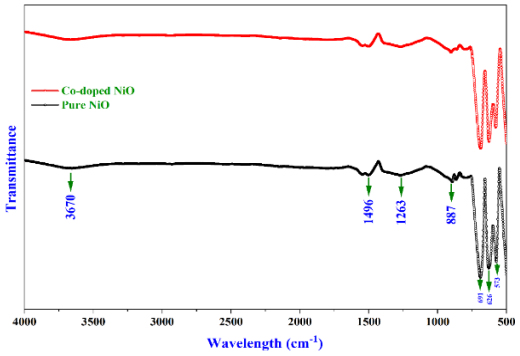

Fig.4 FTIR spectra of both nanoparticles

4. Conclusion

This research validated the successful bio-genic synthesis of NiO and Co-doped NiO nanoparticles using *Hibiscus sabdariffa* fruit extract. Structural analysis confirmed a cubic lattice with a reduced crystallite size upon Co incorporation, while optical studies revealed a narrowing of the band gap from 3.15 to 2.72 eV. The Co-doped NiO nanoparticles exhibited exceptional photocatalytic efficiency, achieving 95.58% degradation of methylene blue, attributed to enhanced light absorption, smaller particle size, and improved charge carrier dynamics. These findings highlight the potential of biogenically synthesized Co-doped NiO nanomaterials as cost-effective and eco-friendly photocatalysts for wastewater treatment and environmental remediation.

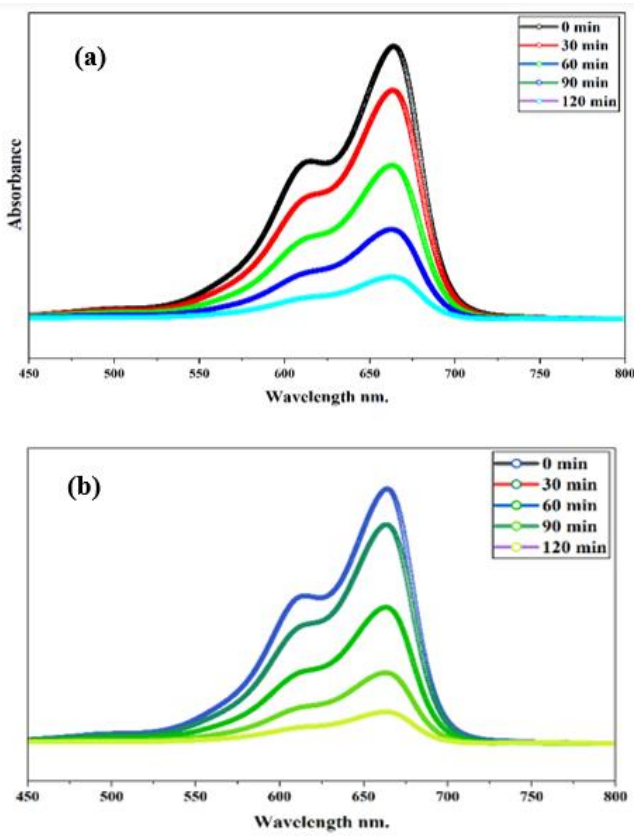

Fig.5 Absorbance graph of a) Pure NiO, b) Co-doped NiO nanoparticles during dye degradation

5. Reference

[1] A. Fakhri, S. Behrouz, M. Asif, I. Tyagi, S. Agarwal, and V. K. Gupta, "Synthesis, structural and morphological characteristics of NiO nanoparticles Co-doped with boron and nitrogen," *J. Mol. Liq.*, vol. 213, pp. 326–331, Jan. 2016, doi: 10.1016/J.MOLLIQ.2015.09.004.

[2] K. Inbarajan and S. Sowmya, "Effectual application of green synthesized Co-doped NiO and Ce:Co-doped NiO nanomaterials in devising photo-cathode for dye-sensitized solar cells," *Ionics (Kiel).*, vol. 30, no. 10, pp. 6719–6728, Oct. 2024, doi: 10.1007/S11581-024-05709-9/TABLES/4.

[3] H. Liu, G. Yan, F. Liu, Y. Zhong, and B. Feng, "Structural, electrochemical and optical properties of NiOxHy thin films prepared by electrochemical deposition," *J. Alloys Compd.*, vol. 481, no. 1–2, pp. 385–389, Jul. 2009, doi: 10.1016/J.JALLCOM.2009.03.015.

[4] B. G. Rao, D. Mukherjee, and B. M. Reddy, "Novel approaches for preparation of nanoparticles," *Nanostructures Nov. Ther. Synth. Charact. Appl.*, pp. 1–36, Jan. 2017, doi: 10.1016/B978-0-323-46142-9.00001-3.

[5] S. Thakur, R. Kumar, N. K. Dhiman, and A. Kumar, "Enhanced photocatalytic performance of Ce-doped NiO nanoparticles synthesized by coprecipitation method," *Hybrid Adv.*, vol. 6, p. 100225, Aug. 2024, doi: 10.1016/J.HYBADV.2024.100225.

[6] S. Agrawal, A. Parveen, and A. Azam, "Microwave assisted synthesis of Co doped NiO nanoparticles and its fluorescence properties," *J. Lumin.*, vol. 184, pp. 250–255, Apr. 2017, doi: 10.1016/J.JLUMIN.2016.12.035.

[7] M. Jothibas, K. Bharanidharan, E. Paulson, M. Elayaraja, B. A. Kumar, and A. Muthuvel, "Effect of co-dopant proportion on the structural, optical and magnetic properties of pristine NiO nanoparticles synthesized by Sol–gel method," *J. Mater. Sci. Mater. Electron.*, vol. 33, no. 2, pp. 907–919, Jan. 2022, doi: 10.1007/S10854-021-07361-9/METRICS.

[8] P. A. Sheena, H. Hitha, A. Sreedevi, and T. Varghese, "Microstructural characterization and modified spectral response of cobalt doped NiO nanoparticles," *Mater. Chem. Phys.*, vol. 229, pp. 412–420, May 2019, doi: 10.1016/J.MATCHEMPHYS.2019.03.033.

[9] M. El-Kemary, N. Nagy, and I. El-Mehasseb, "Nickel oxide nanoparticles: Synthesis and spectral studies of interactions with glucose," *Mater. Sci. Semicond. Process.*, vol. 16, no. 6, pp. 1747–1752, Dec. 2013, doi: 10.1016/J.MSSP.2013.05.018.

[10] T. Tamesgen, M. A. Ameya, G. Sisay, L. Yuanqi, Z. Kai, and T. T. Beyene, "Harnessing the power of S/N-doped NiO nanoparticles through bandgap tuning to achieve enhanced photocatalytic and antibacterial performances," *Sci. Rep.*, vol. 15, no. 1, Dec. 2025, doi: 10.1038/S41598-025-13151-8.

[11] D. Adler and J. Feinleib, "Electrical and Optical Properties of Narrow-Band Materials," *Phys. Rev. B*, vol. 2, no. 8, p. 3112, Oct. 1970, doi: 10.1103/PhysRevB.2.3112.

[12] A. Diha, S. Benramache, and B. Benhaoua, "Transparent nanostructured Co doped NiO thin films deposited by sol–gel technique," *Optik (Stuttg).*, vol. 172, pp. 832–839, Nov. 2018, doi: 10.1016/J.IJLEO.2018.07.062.

[13] B. Sahin, F. Bayansal, M. Yüksel, and H. A. Çetinkara, "Influence of annealing to the properties of un-doped and Co-doped CdO films," *Mater. Sci. Semicond. Process.*, vol. 18, no. 1, pp. 135–140, Feb. 2014, doi: 10.1016/J.MSSP.2013.11.014.

[14] P. M. Ponnusamy, S. Agilan, N. Muthukumarasamy, M. Raja, and D. Velauthapillai, "Studies on cobalt doped NiO nanoparticles prepared by simple chemical method," *J. Mater. Sci. Mater. Electron.*, vol. 27, no. 1, pp. 399–406, Jan. 2016, doi: 10.1007/S10854-015-3767-8/METRICS.

[15] M. E. A. Sakib, M. L. Hasan, H. Roy, M. M. Hasan, and M. M. Ali, "Colocasia esculenta leaf extracted cobalt oxide nanoparticles: A comprehensive investigation of the microstructural, morphological, antibacterial, and photocatalytic activity," *Next Nanotechnol.*, vol. 8, p. 100215, Jan. 2025, doi: 10.1016/J.NXNANO.2025.100215.

[16] N. Chongwilaikasem, P. Sithisarn, P. Rojsanga, and P. Sithisarn, "Green extraction and partial purification of roselle (Hibiscus sabdariffa L.) extracts with high amounts of phytochemicals and in vitro antioxidant and antibacterial effects," *J. Food Sci.*, vol. 89, no. 12, p. 8819, Dec. 2024, doi: 10.1111/1750-3841.17418.

[17] R. Uthrakumar, M. Venkatachalapathy, S. K, N. Rajkamal, C. M, and K. K, "A Study of the Application, Synthesis, and Removal Mechanisms of Co Doped Nio Nanoparticles for Wastewater Treatment," 2023, doi: 10.2139/SSRN.4455431.

[18] G. Bharathy and P. Raji, "Pseudocapacitance of Co doped NiO nanoparticles and its room temperature ferromagnetic behavior," *Phys. B Condens. Matter*, vol. 530, pp. 75–81, Feb. 2018, doi: 10.1016/J.PHYSB.2017.10.106.

[19] K. Varunkumar, R. Hussain, G. Hegde, and A. S. Ethiraj, "Effect of calcination temperature on Cu doped NiO nanoparticles prepared via wet-chemical method: Structural, optical and morphological studies," *Mater. Sci. Semicond. Process.*, vol. 66, pp. 149–156, Aug. 2017, doi: 10.1016/J.MSSP.2017.04.009.

[20] M. S. Wu and W. H. Hsu, "Nickel nanoparticles embedded in partially graphitic porous carbon fabricated by direct carbonization of nickel-organic framework for high-performance supercapacitors," *J. Power Sources*, vol. 274, pp. 1055–1062, Jan. 2015, doi: 10.1016/J.JPOWSOUR.2014.10.133.

[21] M. Alagiri, S. Ponnusamy, and C. Muthamizhchelvan, "Synthesis and characterization of NiO nanoparticles by sol-gel method," *J. Mater. Sci. Mater. Electron.*, vol. 23, no. 3, pp. 728–732, Mar. 2012, doi: 10.1007/S10854-011-0479-6.

[22] K. Jayanthi, S. Chawla, K. N. Sood, M. Chhibara, and S. Singh, "Dopant induced morphology changes in ZnO nanocrystals," *Appl. Surf. Sci.*, vol. 255, no. 11, pp. 5869–5875, Mar. 2009, doi: 10.1016/J.APSUSC.2009.01.032.

[23] K. Vallalperuman, M. Parthibavarman, S. Sathishkumar, M. Durairaj, and K. Thavamani, "Synthesis and characterization of Co and Mn doped NiO nanoparticles," *Korean J. Chem. Eng.*, vol. 31, no. 4, pp. 639–643, Feb. 2014, doi: 10.1007/S11814-013-0286-2/METRICS.

[24] V. Raja, S. K. Puvaneswaran, and K. Swaminathan, "Unique and hierarchically structured novel Co3O4/NiO nanosponges with superior photocatalytic activity against organic contaminants," *Front. Mater. Sci.*, vol. 11, no. 4, pp. 375–384, Dec. 2017, doi: 10.1007/S11706-017-0399-3/METRICS.

[25] R. S. Kate, S. C. Bulakhe, and R. J. Deokate, "Co doping effect on structural and optical properties of nickel oxide (NiO) thin films via spray pyrolysis," *Opt. Quantum Electron.*, vol. 51, no. 10, pp. 1–19, Oct. 2019, doi: 10.1007/S11082-019-2026-2/METRICS.

[26] S. Yousaf *et al.*, "Tuning the structural, optical and electrical properties of NiO nanoparticles prepared by wet chemical route," *Ceram. Int.*, vol. 46, no. 3, pp. 3750–3758, Feb. 2020, doi: 10.1016/J.CERAMINT.2019.10.097.

[27] M. A. M. Khan, R. Siwach, S. Kumar, J. Ahmed, and M. Ahamed, "Hydrothermal preparation of Zn-doped In2O3 nanostructure and its microstructural, optical, magnetic, photocatalytic and dielectric behaviour," *J. Alloys Compd.*, vol. 846, Dec. 2020, doi: 10.1016/J.JALLCOM.2020.156479.

[28] T. V. Thi, A. K. Rai, J. Gim, and J. Kim, "High performance of Co-doped NiO nanoparticle anode material for rechargeable lithium ion batteries," *J. Power Sources*, vol. 292, pp. 23–30, May 2015, doi: 10.1016/J.JPOWSOUR.2015.05.029.

[29] S. Panimalar *et al.*, "Studies of MnO2/g-C3N4 hetrostructure efficient of visible light photocatalyst for pollutants degradation by sol-gel technique," *Surfaces and Interfaces*, vol. 20, p. 100512, Sep. 2020, doi: 10.1016/J.SURFIN.2020.100512.

[30] X. Xin *et al.*, "Effect of synthesis conditions on the performance of weakly agglomerated nanocrystalline

NiO," *J. Alloys Compd.*, vol. 427, no. 1–2, pp. 251–255, Jan. 2007, doi: 10.1016/J.JALLCOM.2006.02.064.

[31] M. A. Shafique *et al.*, "Bandgap engineering of NiO, and enhanced photocatalytic performance by Ca doping," *Optik (Stuttg).*, vol. 267, Oct. 2022, doi: 10.1016/J.IJLEO.2022.169634.

[32] J. Pavlović, N. N. Tušar, and N. Rajić, "The Synthesis and Photocatalytic Efficacy of Distinct Nano-Oxides in the Breakdown of Organic Contaminants," *Catal. 2024, Vol. 14, Page 771*, vol. 14, no. 11, p. 771, Oct. 2024, doi: 10.3390/CATAL14110771.

NOMENCLATURE

D	: Crystallite size, nm
δ	: Dislocation density, nm^{-2}
V	: Unit cell volume, $Å^3$
α	: Absorbance Coefficient, cm^{-1}
υ	: Transition Frequency, Hz
E_g	: Band Gap, eV